ISSN 1330-3651 (Print), ISSN 1848-6339 (Online) https://doi.org/10.17559/TV-20220820194302
Original scientific paper

An ANN Based MPPT for Power Monitoring in Smart Grid using Interleaved Boost Converter

P. Balakishan*, I. A. Chidambaram, M. Manikandan

Abstract: The energy sector is highly concerned about the rapid growth in power utilization which causes an imbalance between supply and demand. A demand-side energy management technique has to be developed to prevent substantial supply-side shortages and improve energy efficiency. The current trend in energy management is to lower the price of electricity without limiting use, instead preferring to minimize power usage during peak hours. To address the issue mentioned earlier and balance the overall system, a flexible and portable system that can serve a wide range of customers is necessary. Hence, a grid-connected hybrid system's improved power monitoring technique is proposed to generate and maintain constant DC voltage. An Artificial Neural Network (ANN) based Maximum Power Point Tracking (MPPT) technique is introduced in the smart grid using an interleaved boost converter to achieve power quality improvement with the aid of the Internet of Things (IoT). The PV voltage is improved with an interleaved boost converter, and optimum reliability is obtained with the aid of the ANN approach. The proposed technique can offer a robust and economical solution for tracking the maximum power, which guarantees regulated output and promotes the extraction of all available power from solar panels. By using a 3φ Voltage Source Inverter (VSI), the hybrid system's output is fed to the grid, and the sensors placed in the IoT module measure the generated power. From the results, it is demonstrated that the PV-based IoT approach aids in the compensation of grid stability, power quality issues, and harmonic reduction in the distribution network.

Keywords: artificial neural network; hybrid grid connected system; internet of things; maximum power point tracking; voltage source inverter

1 INTRODUCTION

Energy consumption is increasing worldwide due to the growing energy demand. Also, global warming, high fossil fuel prices, and associated environmental risks lead to the search for alternative Renewable Energy Sources (RES) in the entire world [1]. RES can meet domestic energy needs while emitting almost no air pollution or greenhouse gases. Hence, an efficient and sustainable RES has to be formulated to meet the everyday energy requirements [2, 3]. Solar energy is regarded as the most intriguing RES because of its permanent and non-polluting nature. One of the most advantageous solar energy systems is the PV system, whose installation is widespread. It can be employed as a stand-alone system or connected to a grid [4]. Depending upon the load, cell temperature, and amount of solar irradiance, the PV panel generates power. Due to these nonlinear characteristics of solar energy, the efficiency of solar array systems varies [5, 6].

The MPPT has the potential to guarantee effective use of solar cells, the mismatch between loads, and supplied maximum power points of PV module. The MPPT algorithms use the current and voltage collected from the PV system to control the duty cycle of the pulse width modulation (PWM) generator [7, 8]. The converter switches receive the generated pulses to regulate their current and voltage. The input voltage acquired from the PV system is increased using different converters, namely boost converter, buck-boost converter, and Cuk converters [9]. In PV applications, boost converters are frequently employed for DC-DC conversion. However, only step-up voltage ratios are effective [10, 11]. The buck-boost converter converts voltage step-up and step-down, but due to its discontinuous input current, it cannot accomplish optimal MPPT without using massive decoupling capacitors [12]. The Cuk converters have continuous input currents and can step up and down voltages.

However, the PV system fluctuates greatly near its maximum power point, thereby restricting the MPPT effectiveness because of their enormous input current ripples [13]. MPPT efficiency enhancement is easier than improving converter efficiency and PV cell conversion ratio. This is made possible by using MPPT algorithms and the Hill Climbing (HC) technique. While determining the MPP, it employs the PV characteristics but is affected by changing atmospheric circumstances [14, 15]. Incremental Conductance (INC), which is regarded as a variant of HC, follows the MPP even when solar radiation fluctuates rapidly. However, the INC requires additional current and voltage sensors which elevate the system's complexity [16]. In such an aspect, the fuzzy logic-based MPPT is introduced to enhance the voltage of the PV module. When the system is in a steady state, the operating point oscillates about the MPP, resulting in the loss of some available energy [17, 18]. Hence, the proposed work attempts to develop an ANN-based MPPT tracking maximum power in PV modules.

Another significant energy source that has the potential to produce reliable energy is wind power. A wind turbine and an electric generator comprise a Wind Energy Conversion System (WECS) [19]. The AC supply obtained from WECS is converted into DC using a rectifier and then applied to the DC link. But, due to its unpredictable nature, wind energy generation follows an irregular pattern. When such irregular sources are integrated with the grid, significant issues occur to grid stability [20]. To solve these issues, monitoring of electricity generated by RES becomes necessary. Thus smart grids are introduced.

A smart grid (SG) is a vast network of wireless devices capable of collecting and sending massive amounts of diverse environmental data in real-time [21, 22]. Smart grids use Information and Communication Technology (ICT) to increase sustainability, quality performance, and demand forecasts while consuming fewer resources. The ICT also assists the intelligent grid in incorporating renewable energy sources. The IoT plays a significant role in an individual's life by enabling the connectivity of numerous physical devices through the internet [23, 24]. The devices are intelligently connected to allow for new types of communication between things and people and between things to exchange data for monitoring and controlling the devices from anywhere in the world using the internet connection. With IoT applications, communication between machines or other devices is

feasible without human interaction [25-28]. The IoT principle's goal is to use wired or wireless nodes to connect the sensors and gadgets of a particular system to a common network. To minimize the hazards associated with wired systems, IoT-based wireless technologies are frequently used [29-32]. Therefore, renewable energy sources use a smart grid based on IoT for effective power monitoring.

This paper proposed an IoT-based SG system to monitor the power generated by hybrid PV-wind energy renewable sources. An interleaved boost converter is introduced to enhance the output voltage of PV. A VSI is used to apply the electricity generated by the hybrid RES to the grid while the IoT device monitors it continuously.

2 PROPOSED CONTROL SYSTEM

The increased consumption of power by people all over the world leads to the introduction of RES, such as solar and wind energy. However, the power generated by these hybrid renewable energy sources has to be monitored to reduce the imbalance between supply and demand. Hence, IoT is utilized for effectively monitoring the power generated by this hybrid system. The block diagram of the proposed system is represented in Fig. 1.

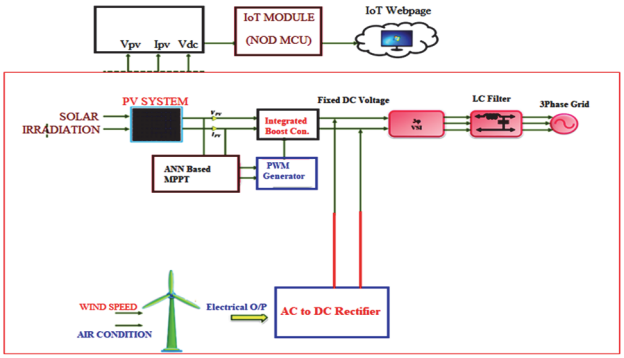

Figure 1 Block diagram of the proposed system

An IoT-based SG system is used to monitor the power generated by hybrid PV-wind energy renewable sources. Initially, the maximum power is extracted from the PV module using an ANN-based MPPT. The maximum current and voltage obtained are then applied to the PWM generator to convert it into a pulse. The interleaved boost converter switches receive the generated pulses to regulate the converter operation. The AC supply obtained from WECS is converted into DC using a rectifier and then it is applied to the DC link. The input and output current obtained from interleaved boost converter and the output obtained from the rectifier are applied to the dc link voltage, which is then converted into AC using VSI. Furthermore, the AC and voltage are filtered using an LC filter and then applied to the grid. Finally, an IoT-based smart grid system is adopted to monitor the obtained AC current and voltage effectively.

2.1 PV Modelling

A current source parallel to a PN junction with an anode linked to a positive terminal represents an ideal PV cell. The equivalent circuit for a single diode PV cell is represented in Fig. 2.

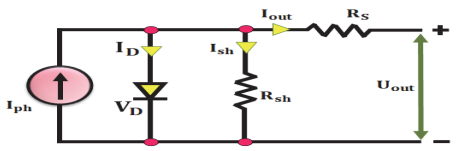

Figure 2 Single diode PV cell equivalent circuit

The single-diode equivalent circuit is assembled using a current source connected in parallel to a forward diode, a resistance connected in parallel, and a resistance connected in series. The PV cell begins to produce electricity as soon as it senses sunlight [1]. The PV cell output current is calculated using Kirchhoff's current law as follows:

$$i_{pv} = i_{ph} - i_d - i_{sh} \tag{1}$$

The photocurrent is denoted as the current flowing across the forward diode, and the current flowing across the shunt resistance is denoted as i_{sh}. When the diode current and shunt resistance current are substituted in Eq. (1) then the appropriate expression is shown in Eq. (2).

$$i_{pv,c} = i_{ph} - i_s\left[\exp\left(\frac{Q\left(V_{Pv} + i_{Pv,c}R_s\right)}{\eta k T_c}\right) - 1\right] - \frac{V_{Pv,c} + i_{Pv,c}R_s}{R_{sh}} \tag{2}$$

where the reverse saturation of diode or leakage current of the electron charge is denoted as "Q", the diode ideality factor is denoted as "η", the Boltzmann constant is denoted as "k" the actual temperature of the cell is denoted as T_c, the cell output voltage is denoted as V_{Pv}, the cell output current is denoted as i_{Pv}, shunt resistance of the cell is denoted as R_{sh} and cell series resistance is denoted as R_s. Furthermore, the output voltage and output current relationship described in (9) are restated as follows when the PV cells are connected in series to form a module:

$$i_{pv,m} = i_{ph} - i_s\left[\exp\left(\frac{Q\left(V_{Pv} + N_s i_{Pv,m}R_s\right)}{N_s \eta k T_c}\right) - 1\right] - \frac{V_{Pv,m} + N_s i_{Pv,m}R_s}{N_s R_{sh}} \tag{3}$$

where, the module current is denoted as $i_{pv,m}$, module voltage is denoted as $V_{Pv,m}$ and the number of PV cell for a module is denoted as N_s. In order to achieve the necessary output voltage and power, the PV modules are connected in series or parallel. The PV modules connected in parallel or series constitute an array. The following describes how Eq. (3) is modified to produce the PV array:

$$i_{pv,m} = i_{ph}N_p - i_s N_p\left[e^{\left(\frac{Q\left(V_{Pv,m} + \frac{N_s}{N_p} i_{Pv,m}R_s\right)}{N_s \eta k T_c}\right)} - 1\right] - \frac{V_{Pv,m} + \frac{N_s}{N_p} i_{Pv,m}R_s}{\frac{N_s}{N_p}R_{sh}} \tag{4}$$

where, the number of cell strings in parallel is denoted as N_p. From Eq. (1), it is inferred that the photocurrent i_{ph} depends on the solar radiation G, the actual cell temperature T_c and the PV cell's surface. Hence, i_{ph} is expressed as follows:

$$i_{ph} = \left(i_{ph,n} + K_1 \Delta T_c\right) \frac{G}{G_N} \tag{5}$$

where, the solar irradiance is denoted as G, the solar irradiance at STC is denoted as G_n, the photocurrent at STC is denoted as $i_{ph,n}$, the short circuit current's temperature coefficient is denoted as K_1 and the fluctuation of actual cell temperature T_c is denoted as ΔT_c. It is clear from Eq. (2), Eq. (3) and Eq. (4), that the diode saturation current i_s depends on cell temperature and it is stated as follows:

$$i_s = i_{sn} \left(\frac{T_c}{T_{c,n}}\right)^3 \exp\left[\left(\frac{Q\left(E_{go}\right)}{\eta k}\right)\left(\frac{1}{T_{c,n}} - \frac{1}{T_c}\right)\right] \tag{6}$$

where the material's (eV) energy band gap is denoted as E_{go}. According to the type of semiconductor material being used, 1.12 eV is selected as the value. The diode saturation current at STC is denoted as $i_{s,n}$. Then, $i_{s,n}$ is stated as follows:

$$i_{s,n} = i_{ph,n} \exp\left(\frac{Q\left(V_{oc,n}\right)}{N_s \eta k T_c}\right) \tag{7}$$

By controlling the voltage slope and current relationship, the series resistance R_s and shunt resistance R_{sh} improves the cell performance. Thus, R_s and R_{sh} are approximated as follows:

$$R_{sh} > \frac{10 V_{oc}}{i_{sh}} \tag{8}$$

$$R_s > \frac{0.1 V_{oc}}{i_{sh}} \tag{9}$$

where, the open circuit voltage is denoted as V_{oc} and short circuit current is denoted as i_{sh}.

2.2 Interleaved Boost Converter

The proposed converter consists of two interleaved and intercoupled boost converter cells and its equivalent circuit is schematically depicted in Fig. 3. With the same winding orientation, the inductors are closely coupled. Hence, an equivalent circuit with three uncoupled inductors is used to represent the coupled inductors.

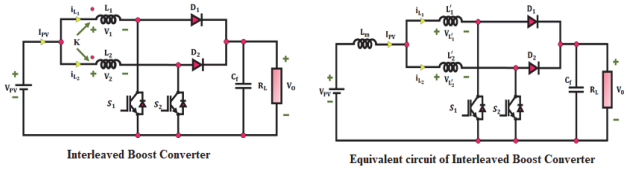

Figure 3 Interleaved Boost Converter and Equivalent circuit

The following equations relate the relationships between the inductors:

$$L'_1 = L_1 - L_m \tag{10}$$

$$L'_2 = L_2 - L_m \tag{11}$$

$$L_m = k\sqrt{L_1 L_2} \tag{12}$$

where, the inductances of two inductors are denoted as L_1, L_2, coupling coefficient is denoted as k, leakage inductances of two inductors in equivalent circuit are denoted as L'_1, L'_2 and mutual inductance is denoted as L_m.

The functioning of the converter is illustrated using the equivalent circuits for the various switching states are discussed below. The functioning of converter in switching "mode 1" and switching "mode 2" is shown in Fig. 4.

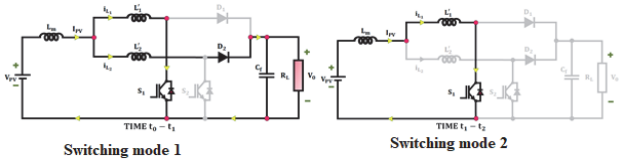

Figure 4 Switching mode of Interleaved Boost Converter

In switching mode 1, SW_1 is closed at time t_0. As the inductor L'_2 continues to discharge, the current L'_1 starts to increase. During the last switching cycle, the current in L'_2 was obtained. The approximate formula for the rate of change of iL'_2 is given by

$$\frac{\mathrm{d}iL_2}{\mathrm{d}t} = \frac{-V_0}{L'_1 + L'_2} \tag{13}$$

In switching mode 2, iL_2 falls to zero at time t_1. The rate of change of iL_1 when it continues to increase is given by:

$$\frac{\mathrm{d}iL_1}{\mathrm{d}t} = \frac{V_1}{L_1} \tag{14}$$

The functioning of converter in switching "mode 3" and switching "mode 4" is shown in Fig. 5.

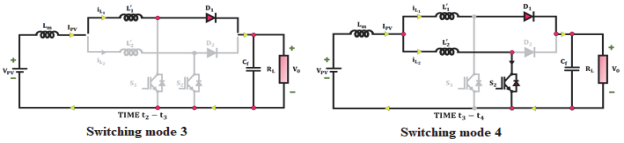

Figure 5 Switching mode of Interleaved Boost Converter

In switching mode 3, SW_1 is opened at time t_2. Through the boost rectifier SD_1, the stored energy of inductor L_1 is delivered to the load. The rate of change of iL_1 is given by:

$$\frac{\mathrm{d}iL_1}{\mathrm{d}t} = \frac{-\left(V_0 - V_i\right)}{L_1} \tag{15}$$

In switching mode 4, SW_2 is closed at time t_3. As the inductor L'_1 continues to discharge, the current L'_2 starts to

increase. The approximate formula for the rate of change of iL_1 is given by:

$$\frac{\mathrm{d}iL_1}{\mathrm{d}t} = \frac{-V_0}{L'_1 + L'_2} \tag{16}$$

The functioning of converter in switching "mode 5" and switching "mode 6" is shown in Fig. 6.

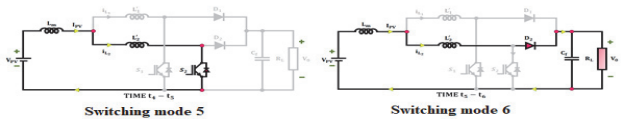

Figure 6 Switching mode of Interleaved Boost Converter

In switching mode 5, iL_2 increases at time t_4.

$$\frac{\mathrm{d}iL_2}{\mathrm{d}t} = \frac{V_i}{L_2} \tag{17}$$

In switching mode 6, SW_2 is opened at time t_5. Through output circuit, the L'_2 discharges. The rate of change of iL_2 is given by:

$$\frac{\mathrm{d}iL_2}{\mathrm{d}t} = \frac{-(V_0 - V_i)}{L_2}$$

When SW is turned on at t_6, the switching cycle will be repeated.

2.3 ANN Based MPPT

Artificial neural networks (ANNs) are a family of statistical learning models that are used to estimate or approximate functions that rely on large number of inputs and are typically unknown. ANNs were inspired by biological neural networks, specifically the central nervous systems of animals, particularly the brain. ANNAs are typically shown as networks of connected "neurons" that communicate with one another. Neural networks are able to adapt to inputs and learn because of the connections adjustable to numerical weights.

The relation shown in Eq. (18) provides the model of a common neuron, where the augment of activation function is denoted as Z:

$$Z = \sum_{m=1}^{M} w_m x_m + \alpha \tag{18}$$

The M incoming signals are denoted as $x_1, x_2, \ldots, x_m$, and the related synapses weights are denoted as $w_1, w_2, \ldots, w_m$. The activation function of linear, threshold and sigmoid transfer functions is given by:

$$y = \frac{1}{1 + e^{-z}} \tag{19}$$

In general, the ANN are seen as a directed graph, where the nodes and edges correspond to the neurons and synapses, respectively. The ANN structure used for the proposed work is multilayer Feed-forward Neural Network (FNN), which is represented in Fig. 7.

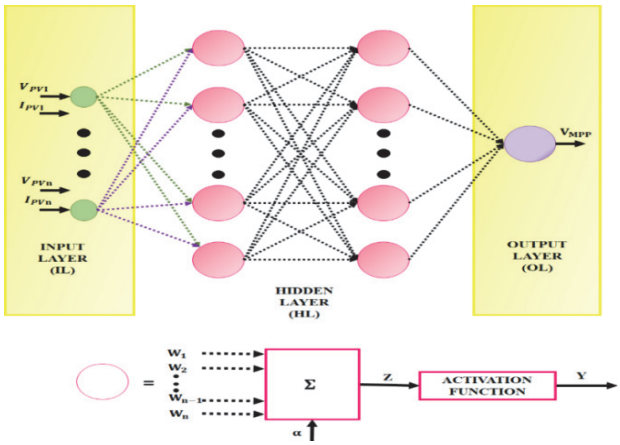

Figure 7 Multilayer Feed-forward Neural Network

The flowchart of proposed ANN based MPPT is shown in Fig. 8.

At the terminals of the PV array, the voltage and current are monitored with a sample time ΔT of a few seconds. Therefore, it is predicted that when the insolation distribution varies, the predicted output power variation ΔP is larger than an acceptable threshold THR. For the proposed ΔT, significant power changes under uniform insolation are impossible.

The former, the ANN method, depends on time (for fixed PV array) and error of training and nonlinear function approximation if the input parameters differ from the data used to train AN. The latter, IncCond method has trade off between tracking time and static error. The combination of two methods solved these problems successfully.

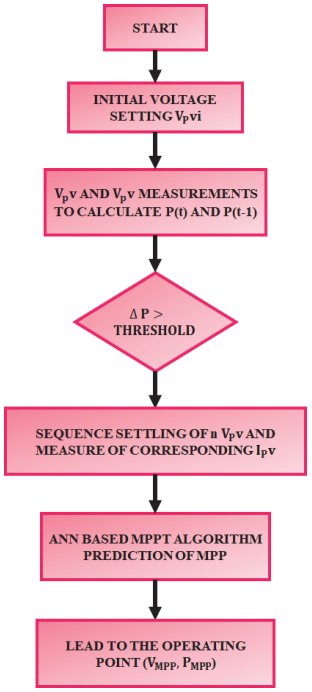

Figure 8 Flow chart of ANN based MPPT

In this method, two stages are used to track MPP of PV array. In the first stage, the trained AN has guided (V_{ref}, I_{ref}) to optimal point (V_{opt}, I_{opt}) which is close to MPP.

The power converter attached to the PV array terminals enables it to consecutively function at n different voltages everytime the suggested ANN based MPPT approach is enabled by altering the resistance perceived by the PV system. The applied voltages and corresponding currents are then measured, and the collected data is gathered by the ANN approach, which offers the voltage that must be adjusted in order to attain the MPP. In other words, V_{Pv} and I_{Pv} constitute the input of the ANN and the PV array voltage V_{MPP} connected to the E_{MPP}, evaluated by the ANN, under the currentoperating circumstances is the output of the ANN. Thus, the power converter applies the working point V_{MPP}, P_{MPP} to the PV array to increase E_{MPP} precision.

2.4 Wind Energy Conversion System (WECS)

The ability of the rotor to run at a variable speed or being forced to work at a constant speed is a key contrast between wind turbines with variable and constant speeds. The frequency of the electrical system determines the speed of the basic generators that are used with constant speed wind turbines. Variable speed wind turbines have the ability to operate at their peak aerodynamic efficiency for a longer period of time than constant speed turbines, despite the higher cost of the power electronics requirement. This is clearly demonstrated if the performance coefficient C_p of wind turbine is against the tip speed ratio.

$$\lambda = \frac{V_{tip}}{V_{wind}} = \frac{\omega R}{\upsilon} \tag{20}$$

where, the blades angular velocity is denoted as ω, rotor radius is denoted as R and wind speed is denoted as v.

All variations in wind speed are sent as variations in mechanical torque, which are subsequently transmitted as variations in the electrical power grid, because constant speed turbines operate at a given speed. This, together with the improved energy collection attained by utilising a variable-speed wind turbine, offers sufficient advantages to make the power electronics economically viable. As a result, designing and building variable-speed wind turbines is the current trend in the wind industry.

2.5 Grid Connected 3φ VSI

A 3φ grid-connected VSI with an LCL filter inserted between the VSI and grid is represented in Fig. 9.

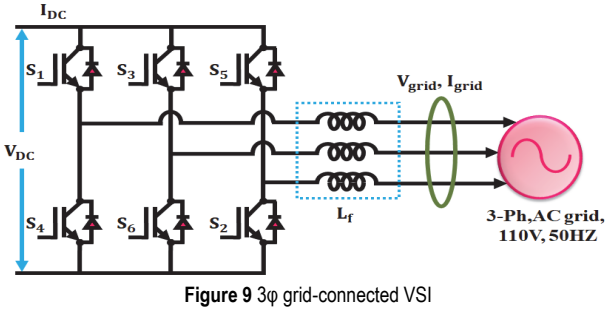

Figure 9 3φ grid-connected VSI

The system's dynamical equations in the stationary frame are provided as follows:

$$\frac{\mathrm{d}i_{1s}}{\mathrm{d}t} = -\frac{r_1}{L_1} i_{1s} + \frac{1}{L_1}\left(V_{is} - V_{cs}\right) \tag{21}$$

$$\frac{\mathrm{d}i_{2s}}{\mathrm{d}t} = -\frac{r_2}{L_2} i_{2s} + \frac{1}{L_2}\left(V_{cs} - V_{gs}\right) \tag{22}$$

$$\frac{\mathrm{d}V_{cs}}{\mathrm{d}t} = \frac{1}{C}\left(i_{1s} - i_{2s}\right) \tag{23}$$

where, the space vectors representing inverter currents are denoted by i_{1s}, grid current is denoted by i_{2s} and capacitor voltages are denoted by V_{cs} respectively. The Eq. (21), Eq. (22) and Eq. (23) are written in matrix form as follows:

$$\frac{\mathrm{d}}{\mathrm{d}t} x = FX + b_s v_i + d_s v_g \tag{24}$$

Where:

$$F = \left[-\frac{r_1}{L_1} 0 - \frac{1}{L_1} 0 - \frac{r_2}{L_2}\frac{1}{L_2}\frac{1}{C} - \frac{1}{C} 0\right], \quad b_s = \left[\frac{1}{L_1} 00\right], \; d_s = \left[-0\frac{1}{L_2} 0\right] \tag{25}$$

When Eq. (24) is converted into the synchronously rotating dq frame, the equations defining the functioning of the system are given by:

$$L_1 \frac{\mathrm{d}i_{1d}}{\mathrm{d}t} + r_1 i_{1d} = \frac{1}{2} u_d V_s - v_{cd} + \omega L_1 i_{1q} \tag{26}$$

$$L_1 \frac{\mathrm{d}i_{1q}}{\mathrm{d}t} + r_1 i_{1d} = \frac{1}{2} u_q V_s - v_{cq} + \omega L_1 i_{1q} \tag{27}$$

$$L_2 \frac{\mathrm{d}i_{2d}}{\mathrm{d}t} + r_2 i_{2d} = v_{cd} - v_{gd} + \omega L_2 i_q \tag{28}$$

$$L_2 \frac{\mathrm{d}i_{2q}}{\mathrm{d}t} + r_2 i_{2q} = v_{cq} - v_{gq} + \omega L_2 i_d \tag{29}$$

$$C \frac{\mathrm{d}v_{cd}}{\mathrm{d}t} = i_{1d} - i_{2d} + \omega C v_{cq} \tag{30}$$

$$C \frac{\mathrm{d}v_{cq}}{\mathrm{d}t} = i_{1q} - i_{2q} + \omega C v_{cd} \tag{30}$$

Where, the control variables are denoted as u_d and u_q, the resistances of L_1 and L_2 are denoted as r_1 and r_2 respectively. Thus, the coupling between the d and q axis components and inverter currents, grid currents and capacitor voltages is evident.

2.6 IoT Based Power Monitoring

In this study, an IoT-based Node MCU controller tracks the electricity generated by a hybrid PV and wind system. The voltage and current sensor are used to monitor the output current and voltage of PV system. The IoT based power monitoring is represented in Fig. 10.

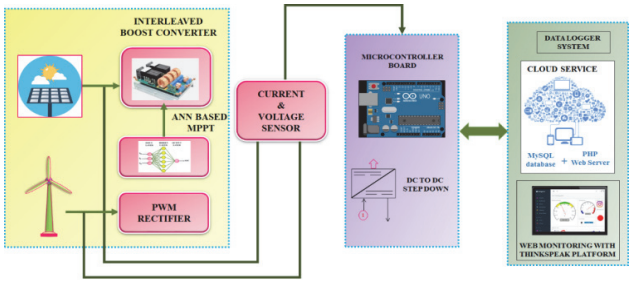

Figure 10 IoT based power monitoring system

The data is collected from the voltage and current sensors are visually displayed using the ThingSpeak platform after being wirelessly uploaded to the cloud server via the IoT protocol. A smartphone or PC is used to access graphic or visual data presentation capabilities remotely and in real-time for continuous data collecting. The proposed system's display unit uses ThingSpeak, an open-source IoT platform as its Application Programming Interface (API). It enables users to gather, store, analyse, visualise, and make choices using sensor data.

3 RESULTS AND DISCUSSION

An IoT based power monitoring system is proposed in this work to monitor the power generated by hybrid PV-wind energy renewable source. An ANN based MPPT is used for tracking maximum power from PV module and to enhance the output voltage of PV, an interleaved boost converter is introduced. A 3φ VSI is used to apply the electricity generated by the hybrid RES to the grid while the IoT device monitors it continuously. The parameter specification of PV system, Interleaved Boost converter and WECS are represented in Tab. 1.

Table 1 Parameter specifications

Parameters	Rating
Peak power	10 KW
Capacity	500 W
Number of panels	20
L_1, L_2	7 mH
C_b	1000 µF
Switching frequency	10 kHz
No. of Wind turbines	1
Power	10 kW
Voltage	575 V
Speed range	4 m/s - 16 m/s

The simulation results obtained by Matlab software for temperature waveform and solar irradiance waveform are represented in Fig. 11.

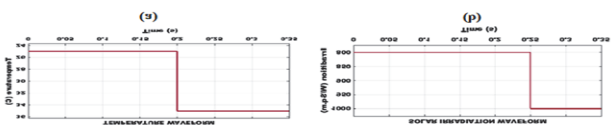

Figure 11 (a) Temperature waveform and (b) Solar irradiance waveform

The temperature waveform clearly demonstrates that the temperature of solar panel is maintained at 25 °C for the first 0.2 seconds. Then, the temperature is raised suddenly and constantly maintained at 35 °C after 0.2 seconds. Likewise, the solar irradiation is maintained at 800 W/sqm for 0.25 seconds, which is increased dramatically to 1000 W/sqm and constantly maintained after 0.25 seconds. The converter input voltage waveform is represented in Fig. 12.

Initially, the output voltage of solar panel is maintained at 281 V at 0.2 seconds, which increases instantly to 291 V at 0.25 seconds. Finally, the voltage is raised immediately to 332 V and maintained constantly after 0.25 seconds. The output voltage and current waveform of interleaved boost converter are represented in Fig. 13.

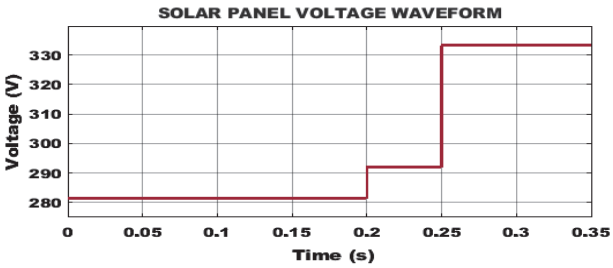

Figure 12 Converter input voltage waveform

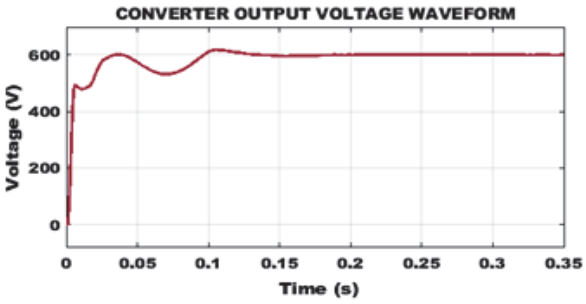

Figure 13 Converter output voltage

The output voltage and current waveform of interleaved boost converter clearly demonstrate that a constant current 600 V is maintained at 0.1 second and voltage of A. Fig. 14 represents the waveforms for the output voltage of the DFIG-based WECS.

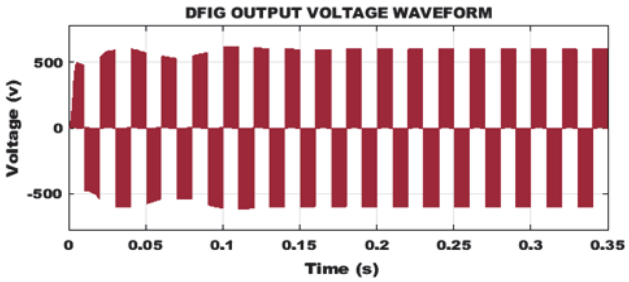

Figure 14 Output voltage waveform of DFIG based WECS

The AC output voltage acquired by the DFIG-based WECS is unstable because of the unpredictable nature of wind. Hence, the output voltage ranges from −500 V to +500 V. The voltage and current waveform of 3φ grid connected VSI is represented in Fig. 15.

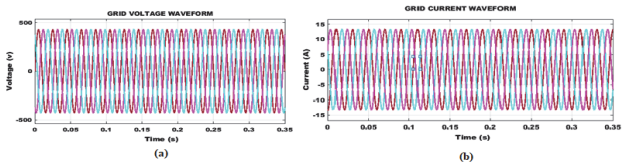

Figure 15 3φgrid connected VSI (a) Voltage (b) Current

The grid voltage and current for 3φ grid connected VSI is obtained without any distortion. The attained grid current value is 450 V and grid voltage value is 13 A. The real and reactive power waveforms of 3φ grid connected VSI is represented in Fig. 16.

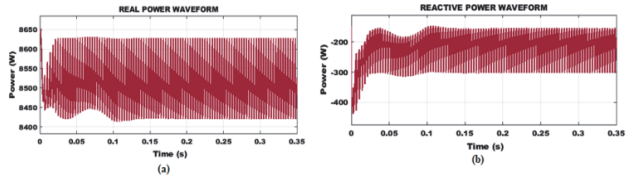

Figure 16 (a) Real power waveform (b) Reactive power waveform

The obtained real power value is about 8630 W and the magnitude of reactive power is found to be low. The attained THD waveform is represented in Fig. 17.

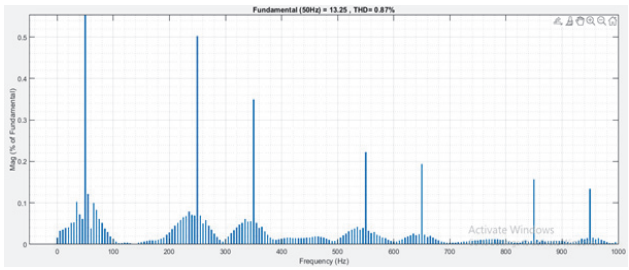

Figure 17 THD waveform

From the THD waveform it is demonstrated that a low THD value of 0.87% is obtained for the proposed methodology.

3.1 Hardware Results

The hardware setup of the proposed methodology is represented in Fig. 18, which consists of 3φ auto transformer, 3φ inverter, inductor, DC-DC converter, PWM rectifier etc.

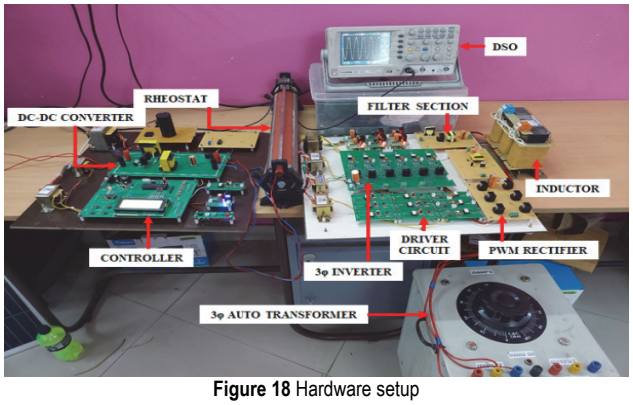

Figure 18 Hardware setup

The different temperature and intensity variations results of DC voltage, AC voltage and current obtained by Adafruit webpage are represented in Fig. 19, Fig. 20 and Fig. 21.

Fig. 19 demonstrates that, at a temperature of 34.3 °C and intensity of 904 W/m^3, the DC voltage, AC voltage and current obtained are 600.2 V, 418.6 V and 3.8 A respectively.

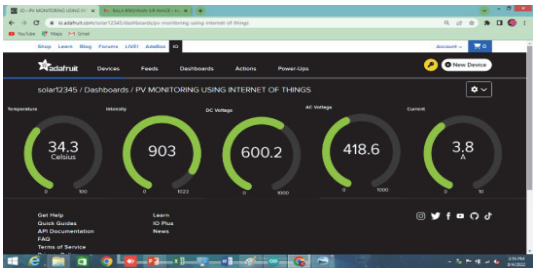

Figure 19 Output of DC voltage, AC voltage and current at different temperature and intensity

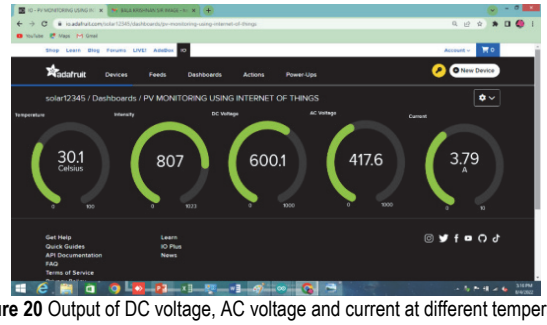

Figure 20 Output of DC voltage, AC voltage and current at different temperature and intensity

Fig. 20 shows that the observed DC voltage, AC voltage and current values are 600.1 V, 417.6 V and 3.79 A at a temperature of 30.1 °C and an intensity of 807 W/m^3.

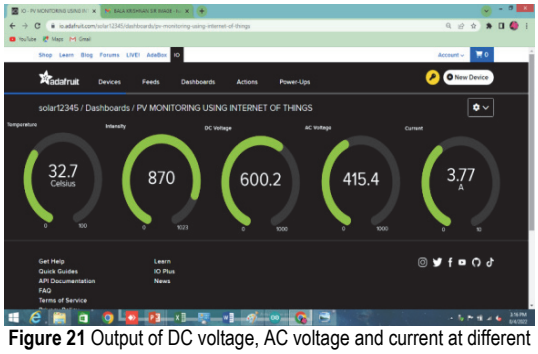

Figure 21 Output of DC voltage, AC voltage and current at different temperature and intensity

Fig. 21 shows that at a temperature of 32.7 °C and an intensity of 870 W/m^3, the resulting DC voltage, AC voltage and current are 600.2 V, 415.4 V and 3.77 A respectively. The comparison of proposed converter with other converters in terms of efficiency and voltage gain are represented in Fig. 22.

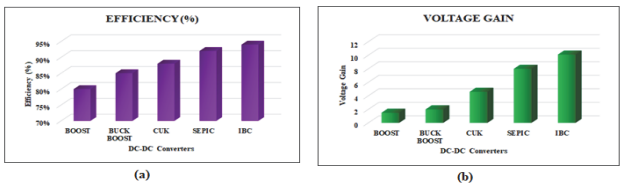

Figure 22 DC-DC Converters (a) Efficiency comparison (b) Voltage gain comparison

By comparing the IBC's efficiency and voltage gain with various other existing converters, the effectiveness of the IBC in improving the performance of the PV system is determined. The proposed IBC has outstanding efficiency of 94% and voltage gain of 1:10 when compared with other converters. The comparison of proposed converter with other existing converters in terms of THD is represented in Fig. 23.

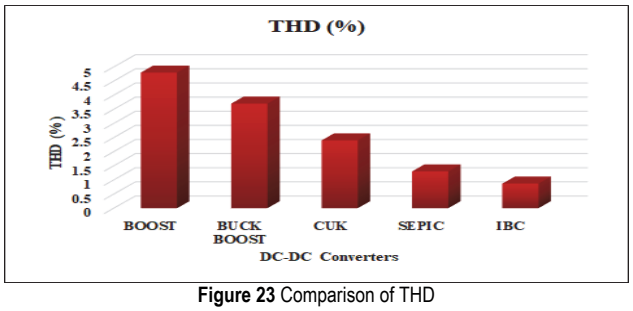

Figure 23 Comparison of THD

The THD comparison of proposed converter with different existing converters demonstrates that the IBC has a low THD value of 0.87%. Hence, the hybrid power system performs better than expected when it comes to reducing power quality problems and boosting microgrid stability.

Table 2 Tracking efficiency of proposed MPPTS.

Irradiation / W/m^2	P_{max}	NeuralNetwork		FuzzyLogic	
		P_{avg}	η_{pv} / %	P_{avg}	η_{pv} /%
650	710.5	710.32	99.73	710.13	99.72
700	761.1	760.42	99.78	760.21	99.81
800	857.2	855.62	99.79	854.62	99.68
900	906.9	904.19	99.77	903.19	99.53
1000	954.7	951.27	99.69	949.4	99.49
1100	1013	1009.2	99.63	1007	99.46

The performance of MPPT techniques can be compared in terms of efficiency. Tab. 2 summarises the simulated results of ANN and FLC controllers. The comparative result with another algorithm like FLC shows that the ANN controller is better and produces more efficiency and stability.

4 CONCLUSION

In this study, an improved power monitoring approach in grid connected hybrid system is introduced to generate and maintain constant DC voltage. An ANN based MPPT technique is introduced in smart grid which obtains maximum power from PV panel. The PV voltage is improved with interleaved boost converter and optimum reliability is obtained with the aid of ANN approach. By using a 3φ VSI, the output of hybrid system is fed to the grid and the sensors placed in IoT module measure the generated power. The voltage and current sensor are used in the monitoring of output current and voltage of PV system. Thus, the power monitoring using IoT facilitates smart power consumption. Also, the reduced THD value of 0.87% proves the effectiveness of the proposed system.

5 REFERENCES

[1] Hassan, F. (2016). Novel high efficiency DC/DC boost converter for using in photovoltaic systems. *Solar Energy*, *125*(6), 22-31. https://doi.org/10.1016/j.solener.2015.11.047

[2] Gustavo, C. G. de M., Igor, C. T., Ícaro, B. Q. de A., Davi, B. B., & Erick, de A. B.. (2021). A low-cost IoT system for real-time monitoring of climatic variables and photovoltaic generation for smart grid application. *Sensors*, *21*(9), 3293. https://doi.org/10.3390/s21093293

[3] Rajvikram. M. E., Gm, S., Sanjeevikumar, P., Nallapaneni, M. K., Annapurna, A., Ajayragavan, M. V., Lucian, M. P., & Jens, B. H. N. (2020). A comprehensive review on renewable energy development, challenges, and policies of leading Indian states with an international perspective. *IEEE Access*, *8*, 74432-74457. https://doi.org/10.1109/ACCESS.2020.2988011

[4] Chuanxiang, X., KazutakaItako, T. K., Keishin, K., & Qiang, G. (2021). Proposal for an Active PV Array to Improve System Efficiency During Partial Shading. *IEEE Access*, *9*, 143423-143433. https://doi.org/10.1109/ACCESS.2021.3121700

[5] Rachid, E., Al-Durra, A., & Muyeen, S. M. (2016). A robust continuous-time MPC of a DC-DC boost converter interfaced with a grid-connected photovoltaic system. *IEEE Journal of Photovoltaics*, *6*(6), 1619-1629. https://doi.org/10.1109/JPHOTOV.2016.2598271

[6] Mojtaba, F., Yanfeng, S., Keyvan, Y., Yam, P. S., & Frede, B. (2017). High-efficiency high step-up DC-DC converter with dual coupled inductors for grid-connected photovoltaicsystems. *IEEE Transactions on Power Electronics*, *33*(7), 5967-5982. https://doi.org/10.1109/TPEL.2017.2746750

[7] Amjad, A., Khalid, A., Sanjeevikumar, P., Vineet, T., Salem, A., Kashif, I., Saiful, I., Md, H. Z., Md, S., & Muhammad, Z. M. (2020). Investigation of MPPT techniques under uniform and non-uniform solar irradiation condition-a retrospection. *IEEE Access*., *8*, 127368-127392. https://doi.org/10.1109/ACCESS.2020.3007710

[8] Srinivasan, V., Boopathi, C. S., Sridhar, R., Mominul, A., Julfikar, H., & Eduardo, M. G. R. (2022). Social Grouping Algorithm Aided Maximum Power Point Tracking Scheme for Partial Shaded Photovoltaic Array. *Energies*, *15*(6), 2105. https://doi.org/10.3390/en15062105.

[9] Kumaran, N., Saikat, G., Yam, S. M., & Teng, L. (2018). A new DC-DC converter for photovoltaic systems: coupled-inductors combined Cuk-SEPIC converter. *IEEE Transactions on Energy Conversion*, *34*(1), 191-201. https://doi.org/10.1109/TEC.2018.2876454

[10] Ferran, R. & Manel, G. (2016). Optimal inductor current in boost DC/DC converters regulating the input voltage applied to low-power photovoltaic modules. *IEEE Transactions on Power Electronics*, *32*(8), 6188-6196. https://doi.org/10.1109/TPEL.2016.2619482

[11] Balaji, C., Chellammal, N., Sanjeevikumarž, P., Mahajan, S. B., Jens, B. H. N., Zbigniew, L., & Samson, O. M. (2020). Non-isolated high-gain triple port DC-DC buck-boost converter with positive output voltage for photovoltaic applications. *IEEE Access*, 8, 113649-113666. https://doi.org/10.1109/ACCESS.2020.3003192

[12] Omar, A. R. & Haoyu, W. (2020). A new high gain DC-DC converter with model-predictive-control based MPPT technique for photovoltaic systems. *CPSS Transactions on Power Electronics and Applications*, *5*(2), 191-200. https://doi.org/10.24295/CPSSTPEA.2020.00016

[13] Divyasharon, R., R. Narmatha, B., & Devaraj, D. (2019). Artificial neural network based MPPT with CUK converter topology for PV systems under varying climatic conditions. *IEEE International Conference on Intelligent Techniques in Control, Optimization and Signal Processing (INCOS)*, IEEE. https://doi.org/10.1109/INCOS45849.2019.8951321.

[14] Claude, B. N. F., Patrice, W., Martin, K., Abderrezak, B., Hyacinthe, T. (2019). Real-time experimental assessment of Hill Climbing MPPT algorithm enhanced by estimating a duty cycle for PV system. *International Journal of Renewable Energy Research*, *9*(3), 1180-1189. https://doi.org/10.20508/ijrer.v9i3.9432.g7705

[15] Eid, A., Gouda, M., Kotb, F., & Dina, A. E. (2019). Modelling and performance analysis for a PV system based MPPT using advanced techniques. *European Journal of Electrical Engineering and Computer Science*, *3*(1). https://doi.org/10.24018/ejece.2019.3.1.47

[16] Mahmoud, N., Ali, K. M., Matti, L., & Mohamed, M. F. D. (2021). An efficient fuzzy-logic based variable-step incremental conductance MPPT method for grid-connected PV systems. *IEEE Access*, *9*. 26420-26430. https://doi.org/10.1109/ACCESS.2021.3058052

[17] Pallavi, V., Rachana, G., & Priya, M. (2020). Asymmetrical interval type-2 fuzzy logic control based MPPT tuning for PV system under partial shading condition. *ISA transactions*, *100*, 251-263. https://doi.org/10.1016/j.isatra.2020.01.009

[18] Mostafa, B., Ahmed, A., Mostafa, A., & Michael, G. (2021). PV systems control using fuzzy logic controller employing dynamic safety margin under normal and partial shading conditions. *Energies*, 14(4), 841. https://doi.org/10.3390/en14040841

[19] Sachin, A., Udaykumar, R. Y., Yellasiri, S., & Angadi, B. R. (2021). Comprehensive review on solar, wind and hybrid wind-PV water pumping systems-an electrical engineering perspective. *CPSS Transactions on Power Electronics and Applications*, *6*(1), 1-19. https://doi.org/10.24295/CPSSTPEA.2021.00001

[20] Djamila, R. (2018). Energy management for PV installations. *Advances in Renewable Energies and Power Technologies, Elsevier*, 349-369. https://doi.org/10.1016/B978-0-12-812959-3.00011-3

[21] Jun, H., Taha, S. U., Masaichi, S., Shuichi, S., Michiyuki, H., & Kenji, O. (2021). Advanced grid integration test platform for increased distributed renewable energy penetration in smart grids. *IEEE Access*, *9*, 34040-34053. https://doi.org/10.1109/ACCESS.2021.3061731

[22] Selvabharathi, D., Tamanna, B., & Daksh, S. (2019). IoT Based Solar Power Management Using Smart Switching. *International Journal of Soft Computing and Engineering*, *8*(11), 3411-3415. https://doi.org/10.35940/ijrte.B1574.0982S1119

[23] Lokesh, B. R. L. R., Rambabu, D., Rajesh, N. A., Prasad, R. D. P., & Gopi, K. (2018). IoT Enabled Solar Power Monitoring System. *International Journal of Engineering & Technology*, *7*(3), 526-530. https://doi.org /10.14419/ijet.v7i3.12.16172

[24] Youssef, C., Hafsa, C., Fatima, C., Fatima, E., Najia, E. (2020). Design and implementation of an intelligent low-cost IoT solution for energy monitoring of photovoltaic stations. *SN Applied Sciences*, *2*(7), 1-11. https://doi.org/10.1007/s42452-020-2997-4

[25] Devesh, K., Gaurav, G., & Yogesh, D. S. (2021). IOT based solar power monitoring system. *Journal of Emerging Technologies and Innovative Research (JETIR*), *8*(9) 250-255. http://www.jetir.org/papers/JETIR2109130

[26] Poushali, P., Parvathy, A. K., Devabalaji, K. R., Joseph, A., Simont, O., Thanikanti, S. B., Hassan, H. A., & Yuvaraj, T. (2021). IoT-based real time energy management of virtual power plant using PLC for transactive energy framework. *IEEEAccess*, *9*, 97643-97660. https://doi.org/10.1109/ACCESS.2021.3093111

[27] Babu, V., Ahmed. K. S., Shuaib, Y. M., Manikandan, M. (2021). Power Quality Enhancement Using Dynamic Voltage Restorer (DVR)-Based Predictive Space Vector Transformation (PSVT) With Proportional Resonant (PR)-Controller. *IEEE Access*, *9*, 155380-155392. https://doi.org/10.1109/ACCESS.2021.3129096

[28] Babu, V., Ahmed, K. S., Shuaib, Y. M., Mani, M. (2021). A novel intrinsic space vector transformation based solar fed dynamic voltage restorer for power quality improvement in distribution system. *Journal of Ambient Intelligence and Humanized Computing*, *7*(1), 173-180. https://doi.org/10.1007/s12652-020-02831-0

[29] Praveen, K. T., Ganapathy, S., & Manikandan, M. (2022). Improvement of voltage stability for grid connected solar photovoltaic systems using static synchronous compensator with recurrent neural network. *Electrical Engineering & Electromechanics*, 2, 69-77. https://doi.org/10.20998/2074-272X.2022.2.10

[30] Sathish, C., Chidambram, I. A., & Manikandan, M. (2022). Reactive Power Compensation in a Hybrid Renewable Energy System through Fuzzy Based Boost Converter. *Problemele Energeticii Regionale*, 1, 10-26. https://doi.org/10.52254/1857-0070.2022.1-53.02

[31] Sanepalle, G. R., Ganapathy, S., & Manikandan, M. (2022). Three Phase Four Switch Inverter Based DVR for Power Quality Improvement With Optimized CSA Approach. *IEEE Access*, *10*, 72263-72278. https://doi.org/10.1109/ACCESS.2022.3188629

[32] Manikandan, M. & Basha, A. M. (2016). ODFF: Optimized Dual Fuzzy Flow Controller Based Voltage Sag Compensation for SMES-Based DVR in Power Quality Applications. *Circuits and Systems*, *7*(10), 2959-2974. https://doi.org/10.4236/cs.2016.710254

Contact information:

Balakishan PADAKANTI, PhD Student
(Corresponding author)
Department of Electrical Engineering,
Annamalai University,
Annamalai Nagar, Chidambaram, Tamil Nadu 608002
E-mail: balakishan1975@gmail.com

Chidambaram. I. A, PhD, Professor
Department of Electrical Engineering,
Annamalai University,
Annamalai Nagar, Chidambaram, Tamil Nadu 608002
E-mail: driacdm@gmail.com

Manikandan MANI, PhD Professor
Department of Electrical and Electronics Engineering,
Jyothishmathi Institute of Technology and Science,
Karimnagar Telangana State, India 505001
E-mail: cm.manikandan@gmail.com